Silicon
https://doi.org/10.1007/s12633-021-01485-7

ORIGINAL PAPER

Influence of Silicon Nitride (Si_3N_4) on Mechanical and Dielectric Properties of a Novel Fused Silica Ceramic Composites

Kishore Kumar Kandi[1] · Gurabvaiah Punugupati[2] · Pagidi Madhukar[2] · C. S. P. Rao[2] · Murthy Chavali[3,4]

Received: 12 September 2021 / Accepted: 15 October 2021

Abstract
Porous fused silica (SiO_2) ceramic composites were fabricated using a novel gel-casting process and the experiments were conducted using Response Surface Methodology (RSM) central composite with face centred design with a six-centre points approach. The process parameters of a gel-casting process such as solid loading (SL), monomer ratio (RM), monomer content (MC) and additive (Si_3N_4) were considered as input parameters and flexural strength (FS), porosity (Por.) and dielectric constant (DE) as response parameters. Single parameter and interaction parameter effects on responses were studied. The effectiveness of derived models was compared with Analysis of Variance (ANOVA) at a 95% confidence level. Statistical analysis proved that input parameters have a critical effect on responses. The derived RSM mathematical models have a higher R2 value (FS 97.62%, Por. 95.12% and DE 95.93%) which shows the critical relation between actual and predicted values. The optimal responses obtained were FS 86.173 MPa, Por. 39.767% and DE 6.949 corresponding parameters process parameters SL 47.95%, additive (Si_3N_4) 10.43 wt%, MC 15 wt% and RM 3.

Keywords Fused silica · Silicon nitride · Gel-casting · Flexural strength · Porosity · Dielectric constant · RSM

1 Introduction

Ceramics are highly concerned for their mechanical characteristics like strength, durability, and hardness. They are used widely in electronic applications such as semiconductors, conductors, insulators, and magnets due to their electrical and magnetic properties. Advanced ceramics have been progressively used in aerospace, automotive engine, defence, construction, biomedical, nuclear industries, chemical, petrochemical, oil/gas, and industrial wear because of their high strength at elevated temperature, good thermal and chemical stability, low density and high wear resistance. Some applications include space shuttle engine components, tank armour, superconductors, and piezoelectric devices [1, 2].

The fusion process is involved in the manufacture of fused silica in the form of silicon dioxide (quartz, sand) from pure silica sand (Wan et al. 2014a) [3]. Currently fused SiO_2 is one of the crucial materials for many engineering and aerospace applications such as radomes, antenna windows, heat shields and crucibles, because of its remarkable and outstanding properties such as resistance to thermal shock and corrosion, a low thermal expansion coefficient, high softening temperature, a low and stable dielectric constant, and excellent chemical inertness (Haris and Welsh, 1973) [4]. These properties suggest that SiO_2 ceramics are an ideal candidate material for high-temperature wave-transparent applications and radomes. However, the comparatively low mechanical strength of sintered SiO_2 ceramics is inadequate to meet the necessity of advanced re-entry vehicles, especially hypersonic spacecraft. To overcome these limitations, additives including h-BN,

✉ Kishore Kumar Kandi
kishorekumar01@gmail.com

✉ Pagidi Madhukar
pmadhu88@gmail.com

✉ Murthy Chavali
ChavaliM@gmail.com

[1] Department of Mechanical Engineering, CVR College of Engineering, Hyderabad, India

[2] Department of Mechanical Engineering, National Institute of Technology, Tadepalligudem, Andhra Pradesh, India

[3] Office of the Dean (Research) & Division of Chemistry, Department of Science, Faculty of Science & Technology, Alliance University, Bengaluru, Karnataka 562106, India

[4] NTRC-MCETRC and 109 Nanocomposites Technologies Pvt. Ltd., Guntur District, Andhra Pradesh 522201, India

Published online: 03 November 2021

Si_3N_4, fibres, and graphene have been utilized as reinforcements to enhance the mechanical strength of ceramics.

Si_3N_4 based ceramics are extensively applied in various industrial fields owing to numerous properties like high hardness, superior corrosion resistance, excellent mechanical and chemical stability, excellent wear resistance, high decomposition temperature, high strength, and toughness, etc. Si_3N_4 is produced by reacting SiCl with NH_3 (Jong, B.W. et al.,1992) [5]. To attain a high extent of quality, components are spark plasma sintered, hot-pressed or reaction sintered as dense parts cannot be produced through direct sintering. At lower temperatures, the bonding of Si_3N_4 particles is attained by the addition of sintering aids which normally encourage liquid-phase sintering. Even at elevated temperatures, Si_3N_4 ceramics upholds their strength.

Currently, numerous manufacturing methods have been established to fabricate both the porous and dense Si_3N_4 ceramics for structural and functional applications (Chen et al., 2010) [6]. These ceramics can be strengthened using a pressure-less sintering process by the addition of a definite quantity of sintering aids at high temperatures (1750–2000 °C). Si_3N_4 may be completely stabilized electrostatically against agglomeration in aqueous slips either at a pH of less than 5 or greater than 9, having either a positive charge or negative charge, respectively (Greil, 1989) [7].

Gel-casting was first developed at Oak Ridge National Laboratory (ORNL) in the 1960s for hard metals and further developed for ceramic materials by combining traditional slip processing with polymer chemistry (Omatete et al., 1991 and Omatete et al., 1997) [8, 9]. The general principle in this process is the ceramic particles suspended are surrounded by a three-dimensional network of cross-linked polymers. For obtaining maximum solid loading typically a dispersant is used which causes the particles in the ceramic slurry to disperse utilizing an electric double layer or steric stabilization. Shrinkage can be minimized during the sintering process and dense ceramics can be obtained by high solid loading. The free-radical reaction leads to the formation of micro-gels of monomer and cross-linker inside the suspension, which eventually combine to form a macro-gel network. The gel network formed inside the suspension holds the particles together collectively to mould a dense green body that is demoldable and takes the form of the mould cavity. Moulds can be made up of metal or plastic materials that are nonporous (Omatete et al., 1991 and Omatete et al., 1997) [8, 9]. Over the conventional forming methods gel-casting has distinct advantages such as near-net-shape fabrication, low contents of organic monomers, high sintered density, and ease of machinability owing to the intensity of homogeneity and high strength (Nojoomi et al., 2014) [10]. The use of non-porous metal or plastic moulds that are reusable makes this process economical (Omatete et al., 1991 and Omatete et al., 1997) [8, 9]. The advantages of components fabricated using gel-casting technique includes defectless, high strength, uniform density and good formability compared to other forming methods. Gel-casting is attractive for producing complex shapes such as radomes, turbine rotors, gears etc.

Wan et al., (2014) [11] fabricated SiO_2 ceramics with high FS, low Por., DE and low dielectric loss by gel-casting using a low-toxicity *N′*, *N*-dimethyl acrylamide (DMAA) gel system. Investigations were done on the properties of green and sintered ceramics, effect solid loading on the rheology of the slurry. The maximum FS obtained for green bodies and sintered ceramics at an SL of 64 vol% and 66 vol% were 15.4 Mpa and 67.4 Mpa. The DE and low dielectric loss obtained at an SL of 64 vol% were 3.27 and 7.82×10^{-4} (at 1 MHz). Wan et al., (2014a) [3] fabricated fused silica ceramics with excellent properties by gel-casting using *N′*, *N*-dimethyl acrylamide, a low toxic gel system. The results were compared with 2-hydroxyethyl methacrylate and toxic acrylamide systems. Investigations were done on the properties such as thermal shock resistance, mechanical and dielectric properties and effects of sintering temperature on the microstructure. The maximum FS was as high as 81.32 Mpa at 1275 °C and after thermal shock at 600 °C, the residual flexural strength was reduced. Excellent properties were obtained at 1250 °C with the similar FS of 67.43 Mpa and 65.45 Mpa (after thermal shock), the DE of 3.34, and the low dielectric loss of 1.20×10^{-3} (at 1 MHz). Wan et al. (2014b) [12] made an attempt using a natural and non-toxic gel, glutinous rice flour as a binder in the gel-casting of SiO_2 glass. It was found that glutinous rice flour performed exceptionally in the gel-casting process. SiO_2 green samples with 3 wt% glutinous rice flours have an FS of 11.87 Mpa and those sintered at 1275 °C has an FS of 40.02 Mpa with a bulk density of 1.75 g/cm^3. Manivannan et al. (2013) [13] used colloidal silica as a binder to develop an aqueous gel-casting for SiO_2 ceramics. It was found that the slurry with a maximum SL of 73 vol% with a viscosity of 0.70 Pa.s is suitable for gel-casting. The maximum FS of green and sintered bodies was found to be 9 Mpa and 65 Mpa with a theoretical density of 88% and 95%. The nano-silica particles of the binder are stuffing the interstitial spots filling the interstitial spots strengthening the mechanical properties in the developed fused silica green body.

Mao et al. (2006) [14] prepared porous silica ceramics by a starch consolidation casting method. Slurries with various fractions of starch were prepared by ball-milling. The bending strength of the sintered samples varied in the range of 10 Mpa-20 Mpa and the low dielectric constant in the range of 2–2.4 with the porosity of 42%–56%. Lin et al. (2016) [15] fabricated silicon oxynitride (Si_2N_2O) based wave transparent material with multilayer structures by a two-step sintering route. The effects of atmosphere and temperature on the properties and microstructure of the materials were studied. It was observed that the disintegration of Si_2N_2O caused the formation

of the multilayer structure. By regulating the disintegration temperature the thickness of β-Si_3N_4 outer layers and the Si_2N_2O inner layer may perhaps be tailored. The FS of the samples sintered at 1800 °C varied in the range of 210 Mpa-236 Mpa, the DE < 4.8 and loss tangent <0.0044. This process allows these ceramic composites to be broadly used as radomes in military applications. Jia et al. (2003) [16] investigated the mechanical properties of two types of hot-pressed fused silica matrix composites, SiO_2 + 5 vol.% Si_3N_4 and SiO_2 + 5 vol.% Si_3N_4+ 10 vol.% C_f. The fracture toughness and ambient strength were significantly enhanced with the addition of Si_3N_4. The fracture toughness increased sharply from 1.22 to 2.4 Mpa.$m^{1/2}$ by incorporating chopped carbon fibres. The maximum FS of two composites at 1000 °C was found to be 168.9 and 130.6 Mpa which were 77.0 and 77.4% higher than their ambient strength, respectively. Zou et al. (2012) [17] prepared porous Si_3N_4 ceramics by gel-casting and pressureless sintering and used these as frames for Si_3N_4–SiO_2 composites. By repeating the sol-gel infiltration and sintering process amorphous SiO_2 of different contents were introduced into porous Si_3N_4 frames. Si_3N_4–SiO_2 composites with enhanced thermal shock resistance and mechanical properties were obtained. The flexural strength, fracture toughness, density and dielectric constant of Si_3N_4–SiO_2 composites were increased from 92.6 Mpa, 1.05 Mpam$^{1/2}$, 1.62 g/cm^3 and 2.65 to 148.1 Mpa, 1.70 Mpam$^{1/2}$, 2.18 g/cm^3 and 3.61 while the porosity decreased from 49.3% to 22% and the dielectric loss is in the range of 3.23 × 10^{-3} to 3.84 × 10^{-3} with the increase of SiO_2 content from 0 to 25.9 vol%. Li et al. (2009) [18] developed a novel process to fabricate a porous Si_3N_4–SiO_2 ceramic composite by combining oxidation-bonding with sol-gel infiltration-sintering.

The mechanical and dielectric properties of porous Si_3N_4–SiO_2 ceramic composite were enhanced by sol-gel infiltration and sintering at 1250 °C. The FS, Por., fracture toughness, Vickers hardness, DE and a dielectric loss were found to be 120 Mpa, 23.9%, 1.4 Mpam$^{1/2}$, 4.1 Gpa, 3.80 and 3.11 × 10^{-3} (at 14 GHz). Ganesh and Sundararajan (2010) [19] prepared dense β-SiAlON–SiO_2 ceramic composites from β-$Si_4Al_2O_2N_6$ and fused silica varying SiO_2 (20, 40, 50, 60, and 80 wt%) by sintering at 1500–1750 °C for 3–4 h. Thin-wall radomes fabricated by hydrolysis induced aqueous gel-casting (GCHAS) have demonstrated green strengths greater than 20 Mpa. An FS of ~140 Mpa, fracture toughness of 4.2 Mpa.$m^{1/2}$, coefficient of thermal expansion of 3.5 × 10^{-6}/°C, Young's modulus of 214 Gpa, hardness of 1390 kg/mm^2, DE of 5.896 and tangent loss of 0.002 at 17 GHz was exhibited by silicon oxynitride formed from a powder mixture of 60 wt% β-$Si_4Al_2O_2N_6$ and 40 wt% SiO_2 sintered at 1750 °C for 3 h.

RSM is defined as "a collection of mathematical and statistical techniques useful for the modelling and analysis of problems in which a response (output variable) of interest is influenced by several variables (input variables) and the goal is to optimize the responses that are influenced by the input process parameters" (Montgomery, 2012) [20]. Originally, RSM is developed to model experimental responses and then migrated into the modelling of numerical experiments (Box and Draper, 1987) [21]. They can be applied for modelling and optimization of any engineering problems. Sufficient data is gathered through the experimental design layout and numerical models for the required outputs as a function of input parameters were established by utilizing the multiple objective optimizations on the results [22].

2 Materials and Methods

Commercially available SiO_2 (M/s. Ants Ceramics Pvt. Ltd., Thane, India) with an average particle size of 1–5 μm and Si_3N_4 (M/s. Denka Company Ltd., Japan) with an average particle size of <10 μm are used in this study. Deionized water is used as a solvent. Commercially available dispersants such as Darvan 821A and Darvan C-N (both R.T Vanderbilt, Norwalk, CT), Dolapix A88 and Dolapix CE64 (both Zschimmer & Schwarz, Lahnstein, Germany) are used for dispersing ceramic particles in slurries for obtaining high SL and low viscosity. In the process of gel-casting Methacrylamide and *N, N′*- methylene bisacrylamide (both Alfa Aesar United Kingdom) was used as the organic monomer and cross-linker respectively. Ammonium persulfate (APS) and *N, N, N′, N′*-Tetramethyl ethylenediamine (TEMED) (both Alfa Aesar, United Kingdom) are used as the initiator and catalyst. Surface exfoliation phenomenon green samples cast in the air were removed by adding Polyethylene glycol 400 (Alfa Aesar, United Kingdom). Diluted Nitric acid and Ammonium hydroxide (both are from S.D. Fine Chemicals, India) was used for pH adjustment.

3 Slurry Preparation

Figure 1 shows the manufacturing method used for the fabrication of SiO_2 ceramic composites. Ceramic composites were fabricated by varying SL, MC, RM and additive. Primarily the premix suspension was made by the addition of dispersant Darvan 821A (1 Wt% MC), PEG (surfactant), monomers MAM and MBAM (10–15 wt% of solid loading) in distilled water. The liquid suspension was mixed using a magnetic stirrer. The premix solution was mixed with SL of necessary vol% of SiO_2 and Si_3N_4 and stirred for more than 6 h. The trapped air in the solution was eliminated using a deaerator for 10–15 min and later initiator APS (1 wt% of MC) and TEMED were mixed to start polymerization and solidification. The slurry was dispensed into a glass mould and after polymerization, the green bodies were demoulded. The green bodies were dried under controlled humidity conditions for

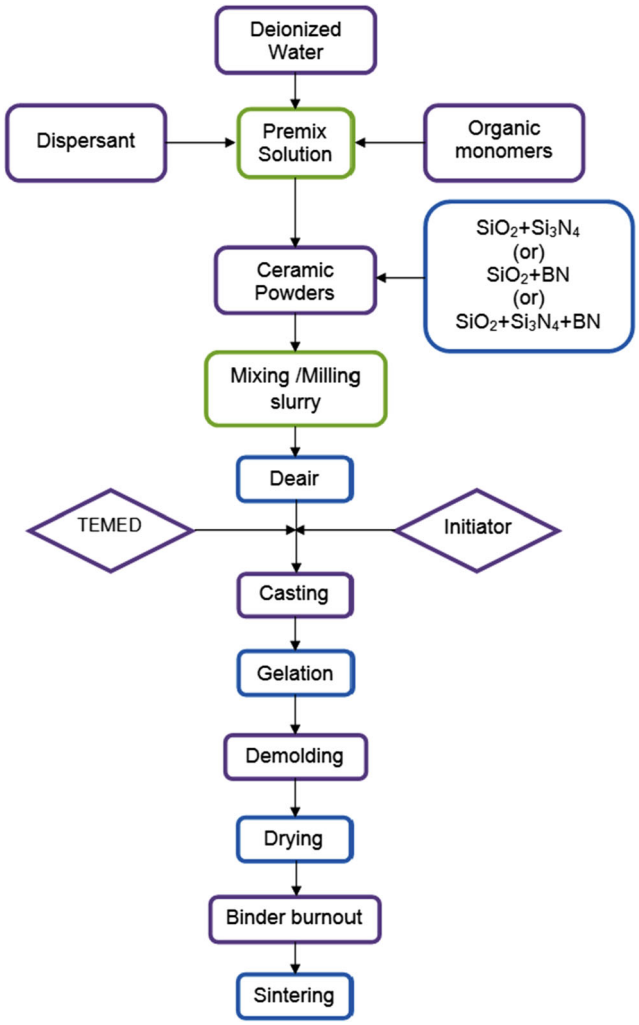

Fig. 1 A detailed flowchart of the gel-casting process of concern ceramic composite

24 h. The binders were burnt at 600 °C in a high temperature muffle furnace for 1 h with a heating rate of 2 °C/min. The sintering method for ceramic samples was conducted in the nitrogen (N_2) environment at 1250 °C with a ramp rate of 4 °C/min. Sintered samples of SiO_2-Si_3N_4 ceramic composites were shown in Fig. 2.

4 Characterization

4.1 Flexural Strength

Flexural strength (Modulus of Rupture) is defined as "the ability of the material to withstand bending forces applied perpendicular to its longitudinal axis". The FS was determined by the three-point flexural method as shown in Fig. 3 with a span length of 40 mm and at a crosshead speed of 0.5 mm/min using a universal testing machine as per ASTM-C1161-02C (2006) and is determined as given in Eq. 1.

Fig. 2 Sintered samples of SiO2-Si3N4

$$\sigma_f = \frac{3PL}{2bh^2} \tag{1}$$

where P = fracture load, L = length of support span, b = width of the sample and h = height of the sample.

4.2 Bulk Density and Apparent Porosity

Bulk density is defined as "the ratio of mass to the volume that includes the cavities in a porous material".

$$BD = \frac{DW}{SW_1 - SW_2} X\ \rho \tag{2}$$

Apparent porosity is defined as "the ratio of open pore volume to total volume"

$$AP = \frac{SW_1 - DW}{SW_1 - SW_2} X\ 100 \tag{3}$$

where BD = Bulk Density, AP = Apparent porosity, DW = Dry Weight, SW_1 = Soaked Weight, SW_2 = Suspended weight, ρ= Density of kerosene oil = 0.78 g/cc.

Bulk density and apparent porosity of ceramic samples were determined by Archimedes principle as per ASTM C373–88(2006) using kerosene as solvent. The specimens were cut into 20 × 20 × 8 mm in size. *Archimedes principle* states that "when an object is partially or fully immersed in a fluid it experiences an upward force that is equal to the weight of the fluid displaced by it".

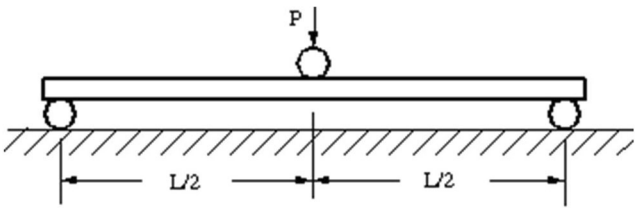

Fig. 3 Schematic of three-point bending

4.3 Dielectric Constant and Loss Tangent

The dielectric constant is defined as "a quantity measuring the ability of a substance to store electrical energy in an electric field". The dielectric constant can be calculated by Eq. 4 by measuring the capacitance:

$$K = \epsilon_r^{'} = \frac{cd}{A} = \frac{\varepsilon}{\varepsilon_0} \tag{4}$$

Where K is the dielectric constant; $\varepsilon_r^{'}$ is relative permittivity, c is the capacitance; d is the thickness of the specimen; A is the area of the cross-sectional surface; ε is the permittivity of the medium; ε_0 is the permittivity of free space or vacuum.

5 Results and Discussion

5.1 Zeta Potential and pH Value

The zeta potential of SiO_2-Si_3N_4 particles in the slurry is studied by varying the dispersant (Darvan 821A) in the range of 0–0.75 wt% as a function of pH value and is depicted in Fig. 4.

The zeta potential of SiO_2–Si_3N_4 slurries without dispersant is found to vary from 5.3 mV at pH 1 to −29.5 mV at pH 11. It can be observed that the isoelectric point (IEP) is at pH 3.8 and the absolute value of zeta potential enhances as pH value increases. It is also observed that the addition of 0.5 wt% Darvan 821A provides the extreme value of zeta potentials which is about −53.5 mV at pH 11, which is the greatest fit for getting fine dispersed SiO_2–Si_3N_4 slurries. The other dispersant levels having good zeta potential except 0.5 wt% Darvan 821A are 0.75 wt% Darvan 821A and 0.25 wt% Darvan 821A. The corresponding zeta potential values are −43.2 mV and − 42.3 mV at pH 11 respectively. The zeta potentials of the residual slurries are found to be lesser and hence not considered.

The pH value of slurry also plays a significant role in the rheological characteristics. It is witnessed that a high absolute zeta potential value is got by raising the pH value of the slurry which increases the dispersibility of the slurry. The development of a hydroxide layer on the surface of SiO_2 particles is eliminated by the addition of Si_3N_4 particles.

5.2 Solid Loading

Higher SL of SiO_2–Si_3N_4 slurry is necessary to enhance the mechanical characteristics of gel-cast parts. The SL of the slurries are altered from 42 to 50 vol% in which Si_3N_4 content varies from 5 to 15 wt% and the remaining is SiO_2. But viscosity improves as the SL increases due to agglomeration at higher SL which makes the slurry tough to pour into a mould for casting. The reason is due to flocculation and coagulation produced by the drop in the amount of solvent (water) existing between the ceramic particles. Therefore, slurry with 50 vol% SL and 15 wt% Si_3N_4 content is fit for casting into the mould. The variation of viscosity as a function of the shear rate ranging from 0.1–100 s^{-1} for slurries of 50 vol% solids loading and with Si_3N_4 content varying from 5 to 15 wt% is presented in Fig. 5.

From Fig. 5 it is observed that there is an increment in viscosity from 0.706 to 0.842 Pa.s with an increase in Si_3N_4 content from 5 to 15 wt% and the gel exhibits shear-thickening behaviour. The increment in viscosity is due to the agglomeration at high SL.

5.3 X-Ray Diffraction Analysis and Microstructure

X-ray diffraction patterns of SiO_2–Si_3N_4 ceramic composite sintered at various temperatures are shown in Fig. 6. X-ray

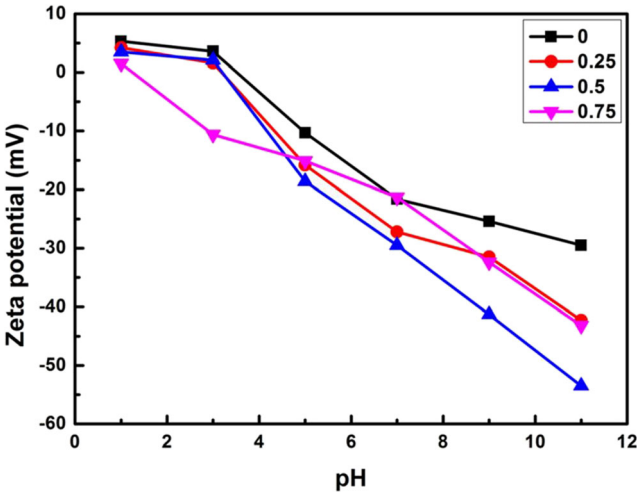

Fig. 4 Zeta potential of SiO2-Si3N4 slurries with dispersant Darvan 821A

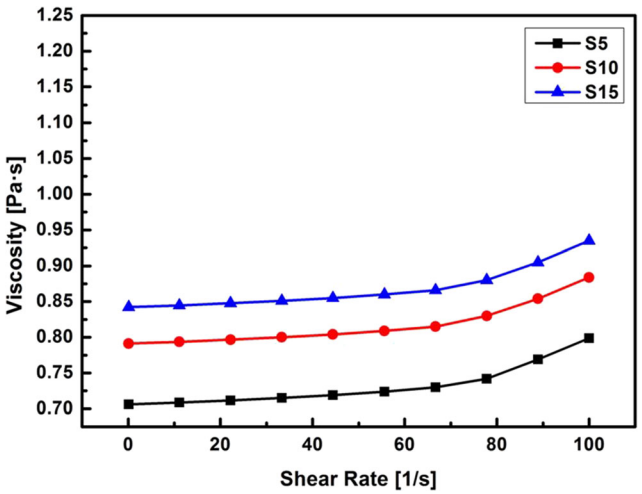

Fig. 5 Variation of the viscosity of slurries at various solid loadings

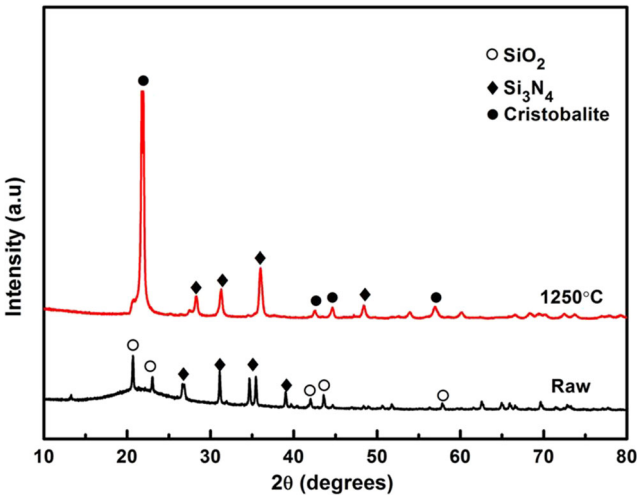

Fig. 6 XRD patterns of SiO2-Si3N4 ceramic composite

diffraction analysis is done both on raw ceramics and ceramic composite sintered at 1250 °C. It can be understood that at 1250 °C, SiO_2 is transformed into a cristobalite phase.

The microstructure of sintered SiO_2-Si_3N_4 ceramic composite is shown in Fig. 7.

5.4 Results and Analysis of SiO_2–Si_3N_4 Ceramic Composites

5.4.1 Regression Model for Flexural Strength

A regression model for FS of SiO_2–Si_3N_4 ceramic composite is fitted using the experimental results. ANOVA has been used on the results for FS and the ANOVA results are presented in Table 1.

Where A is SL, B is Si_3N_4 content, C is MC and D is RM.

From the above results, it has been found that SL, Si_3N_4, MC, RM, and SL^2, are important model terms, and the response of each are shown in Figs 8a, b, c and d respectively. The regression model developed for FS was given in Eq. 5 in the coded form.

$$FS = 80.60 + 13A + 4.16B + 1.23C + 1.37D - AB - 0.73BC - 3.82A^2 + 1.19C^2 \quad (5)$$

From Fig. 8a and b, it is found that FS increases with SL and Si_3N_4 content. Micro-cracks occur in green bodies when the solid loading is low. This may be due to the increase of drying and sintering shrinkages as the space between the particles in the slurry is huge. At low solids loading and Si_3N_4 content the density of the composite decreases during sintering. Therefore, the FS of porous SiO_2–Si_3N_4 sintered ceramic composite is low at lower SL and higher the SL increases the FS. During sintering, the monomers are burnt out leaving pores. Few pores in the composite will be replaced by the cristobalite which is formed during the sintering. Hence, there is a little significant effect of MC and MR on the FS of SiO_2–Si_3N_4 ceramic composites as shown in Fig. 8c and d.

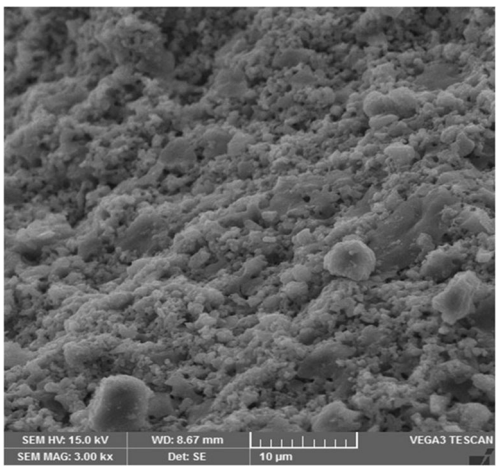

Fig. 7 SEM micrograph of sintered SiO2–Si3N4 ceramic composite

5.4.2 Regression Model for Porosity

A regression model for the porosity of SiO_2–Si_3N_4 ceramic composite is fitted using the experimental results. ANOVA has been utilized on the experimental data for porosity and the ANOVA results are presented in Table 2.

Where A is SL, B is Si_3N_4 content, C is MC and D is RM.

From the above results, it is found that SL, MC, RM, the interaction of MC and RM, $Si_3N_4{}^2$, and RM^2 are significant model terms, and the response of each is shown in Fig. 9a, b, c, d and e. The regression model developed for Por. was represented in Eq. 6, in the coded form.

$$Por. = 37.06 - 2.42A - 0.016B - C - 0.69D - 0.45AB + 0.22AC + 0.15AD - 0.53CD - 0.86A^2 - 1.87B^2 + 0.26C^2 + 1.61D^2 \quad (6)$$

In Fig. 9a, it can be seen that the Por. of the sintered body decreases with the increase in SL. The ceramic particles are compacted, reducing the pores in the composite with an increase in SL. This densifies the ceramic composite. From Fig. 9b, it is observed that Si_3N_4 content has an important influence on the Por. As the Si_3N_4 content increases there is a rise in the porosity and then declines on further addition of Si_3N_4 powder. The rise in the porosity is due to the loose packing of Si_3N_4 particles in SiO_2 ceramics. As the content of Si_3N_4 powder increases the pores in the composite are reduced that increases the density of the composite causing the lower porosity.

Table 1 ANOVA results for flexural strength

Source	Sum of Squares	df	Mean Square	F Value	p value Prob>F	Percentage Contribution
Model	3496.603	8	252.9297	44.09247	< 0.0001	97.598
A-SL	3042.520	1	3042.52	530.3934	< 0.0001	84.924
B-Si_3N_4	311.951	1	311.7505	54.34652	< 0.0001	8.707
C-MC	39.232	1	27.2322	4.747308	0.0457	1.095
D-RM	36.620	1	33.62	5.860874	0.0286	1.022
AB	15.980	1	15.98001	2.785747	0.1158	0.446
BC	8.883	1	8.482656	1.478756	0.2428	0.248
A^2	37.723	1	37.72255	6.576059	0.0216	1.053
C^2	3.696	1	3.695539	0.644232	0.4347	0.103
Residual	86.045	21	5.736346			2.402
Cor Total	3582.649	29				100.00

R-Square: 97.62% Adjusted R-square: 95.41% Predicted R-square: 92.39%

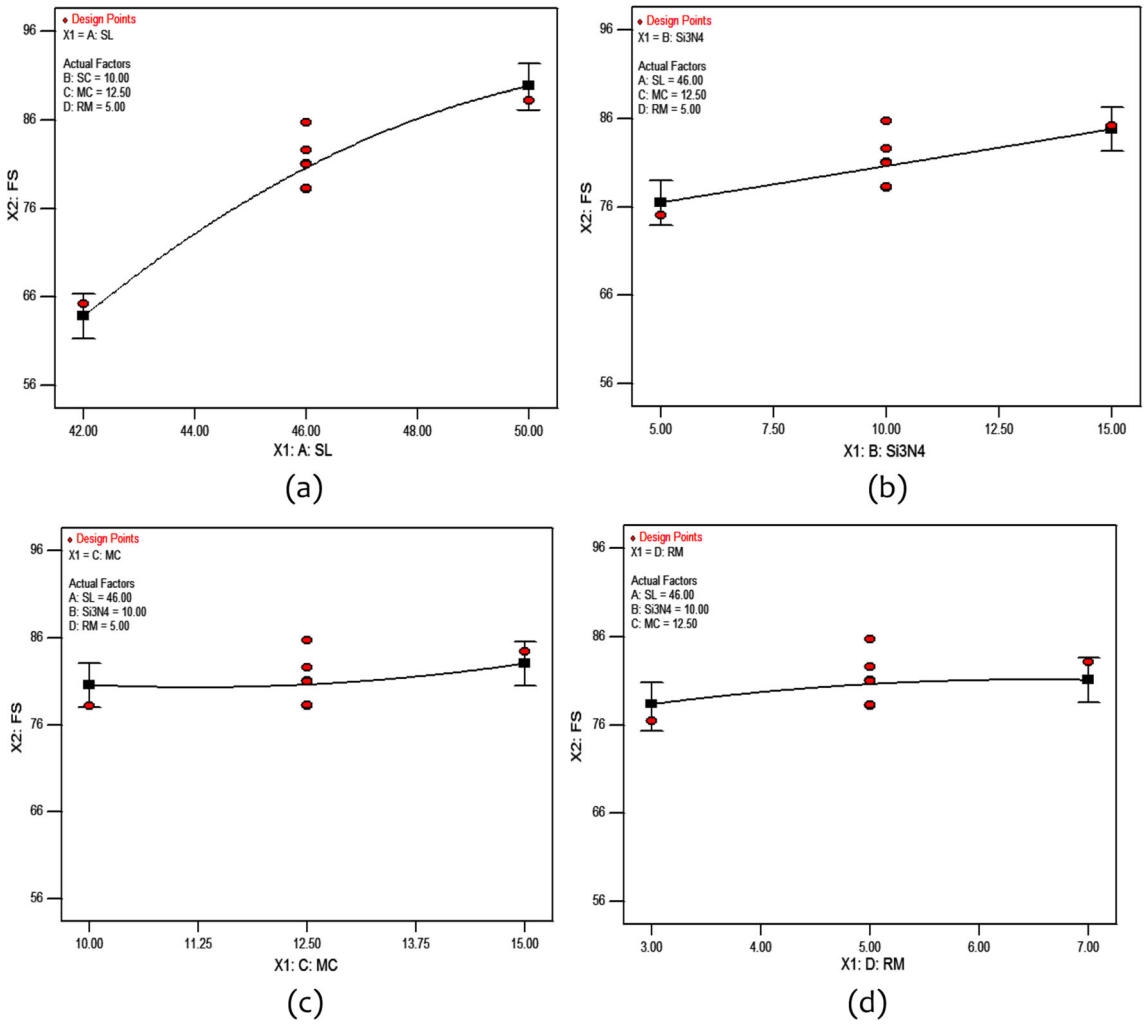

Fig. 8 Influence of process parameters on flexural strength - (**a**) Influence of SL on FS, (**b**) Influence of Si3N4 on FS, (**c**) Influence of MC on FS, and (**d**) Influence of RM on FS

Table 2 ANOVA results for porosity

Source	Sum of Squares	df	Mean Square	F Value	p value Prob>F	Percentage Contribution
Model	158.6867	12	13.22389	27.62487	< 0.0001	95.122
A-SL	105.009	1	105.6089	220.6183	< 0.0001	62.946
B-Si3N4	0.00436	1	0.004356	0.009099	0.9251	0.003
C-MC	17.8802	1	17.8802	37.35197	< 0.0001	10.718
D-RM	8.55601	1	8.556006	17.8736	0.0006	5.129
AB	3.26706	1	3.267056	6.824922	0.0182	1.958
AC	0.79656	1	0.796556	1.664016	0.2143	0.477
AD	0.34516	1	0.345156	0.721036	0.4076	0.207
CD	4.54756	1	4.547556	9.499903	0.0068	2.726
A^2	1.9225	1	1.922496	4.016119	0.0613	1.152
B^2	9.07376	1	9.073755	18.95519	0.0004	5.439
C^2	0.17326	1	0.17326	0.361942	0.5554	0.104
D^2	6.74593	1	6.745934	14.09234	0.0016	4.044
Residual	8.13782	17	0.478695			4.878
Cor Total	166.8245	29				100.00

R-Square: 95.12% Adjusted R-square: 91.67% Predicted R-square: 82.75%

The Por. of the sintered body increases with MC as shown in Fig. 9c. The pores of the sintered body largely initiate from the leftover micro-space of the organic polymers in the green sample during organic binder burnout. The distribution and intensity of pores depend on MC. Thus more the monomer content is more is the porosity in the ceramic body. Figure 9d show the decrease in porosity with the increase of monomers ratio. Higher porosity is obtained on further increase in the monomer ratio. The increase in the ratio of monomers to cross-linker sometimes initiates micro-crack propagation that causes higher porosity. The interaction effects of MC and MR can be seen in Fig. 9e.

5.4.3 Regression Model for Dielectric Constant

A regression model for the dielectric constant of SiO_2–Si_3N_4 ceramic composite is fitted using the experimental results. ANOVA has been implemented on the test data for DE and the ANOVA results are presented in Table 3.

Where A is SL, B is Si_3N_4 content, C is MC and D is RM.

From the above results, it has been found that SL, MC, RM, SL^2, $Si_3N_4{}^2$, RM^2, interactions of Si_3N_4 and RM, and interactions of Si_3N_4, MC and RM are important model terms, and are shown in Fig. 10a, b, c, d and e. The regression model generated for the dielectric constant was represented in Eq. 7, in the coded form.

$$DE = 7.40 + 0.04A + 5.556 \times 10^{-3}B - 0.14C + 0.073D + 0.068BD + 0.26A^2 + 0.26B^2 - 0.12C^2 - 0.37D^2 \quad (7)$$

Figure 10a show the increase in density of SiO_2–Si_3N_4 ceramic composite with the increase in solid loading. This will lead to the reduction of pores that causes the increase of the dielectric constant. From Fig. 10b, it can be found that the DE initially decreases when Si_3N_4 content is in the range of 5 wt% to 10 wt%. This is due to the increase in the surface area of pores. There is a growth in the DE on further increasing the Si_3N_4 content from 10 wt% to 15 wt%. This may be due to the increase in the density of the ceramic composite which reduces the transfer of electromagnetic waves through it.

In Fig. 10c, as the monomer content increases the DE decreases monotonically. The increment in monomer content decreases the density of sintered ceramic due to the formation of large pores during binder burnout. Thus an increase in the monomer content will lower the density and DE of ceramics. In Fig. 10d, it can be seen that the DE increases as the ratio of monomers increase from 3 to 5. This increase is due to the higher binding effect between the ceramic particles that leads to low pores. Further the dielectric constant decreases as the monomer ratio increases from 5 to 7, due to the excessive binding effect, agglomeration of ceramic particles takes place followed by the formation of microcracks. The interaction effects of Si_3N_4 content and RM on DE can be seen in Fig. 10e.

5.4.4 Multi-Objective Optimization Using Desirability Function

Multi-response optimization using the desirability function was carried out in combination with RSM to surmount the

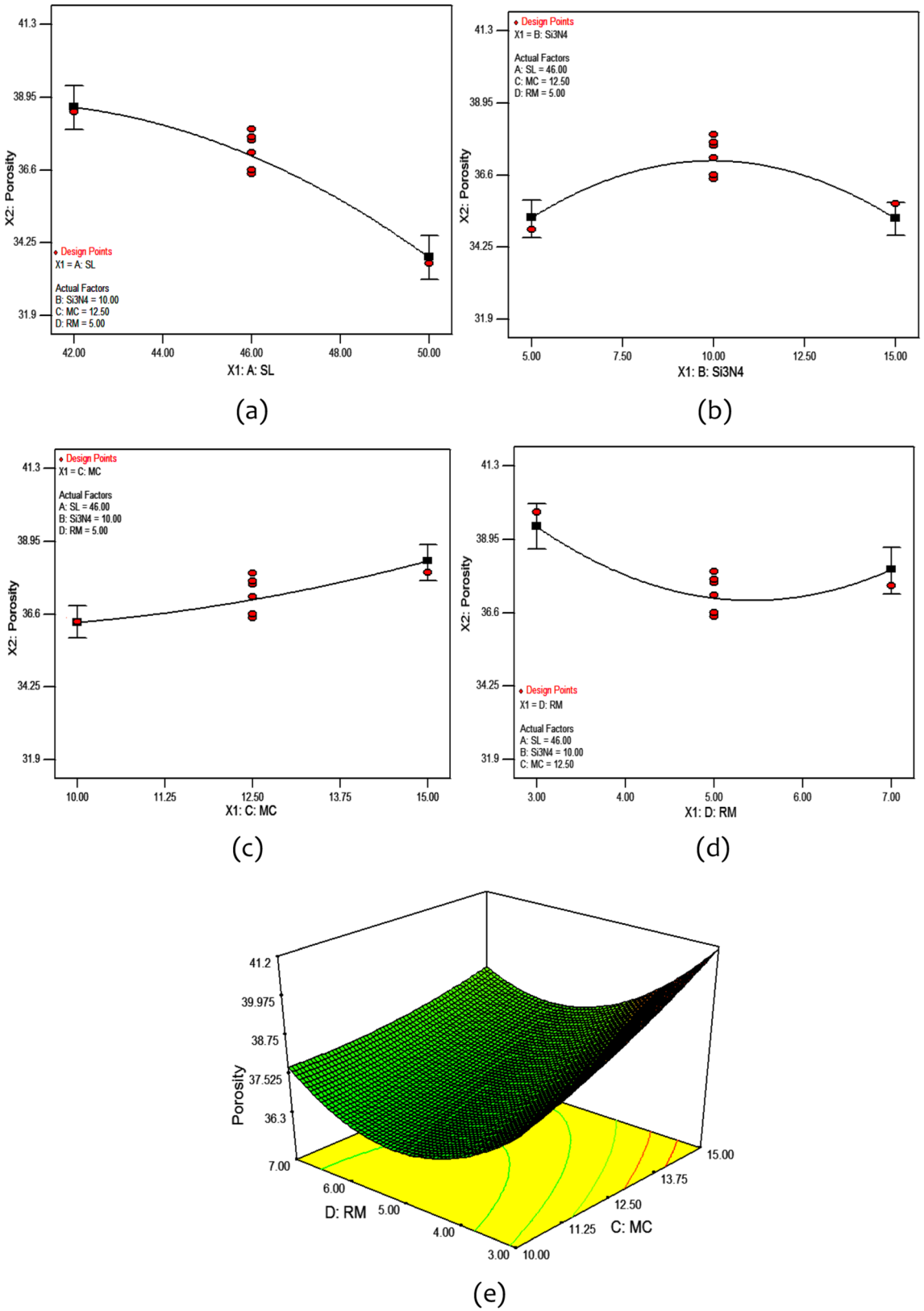

Fig. 9 Influence of process parameters on porosity - (**a**) Influence of SL on porosity, (**b**) Influence of Si3N4 on porosity, (**c**) Influence of MC on porosity, (**d**) Influence of RM on porosity, and (**e**) Influence of MC and RM on porosity

Table 3 ANOVA results for dielectric constant

Source	Sum of Squares	df	Mean Square	F Value	p value Prob>F	Percentage Contribution
Model	4.100	9	0.350244	33.45971	< 0.0001	95.840
A-SL	2.950	1	3.05045	291.4172	< 0.0001	68.969
B-Si3N4	0.001	1	0.000556	0.053074	0.8205	0.013
C-MC	0.339	1	0.338939	32.37969	< 0.0001	7.923
D-RM	0.097	1	0.0968	9.247549	0.0074	2.263
BD	0.074	1	0.074256	7.093888	0.0164	1.736
A^2	0.171	1	0.1708	16.31696	0.0009	3.993
B^2	0.178	1	0.177517	16.95865	0.0007	4.150
C^2	0.039	1	0.039355	3.759641	0.0693	0.920
D^2	0.251	1	0.35134	33.56438	< 0.0001	5.875
Residual	0.178	20	0.010468			4.160
Cor Total	4.278	29				100.00

R-Square: 95.93% Adjusted R-square: 93.07% Predicted R-square: 87.36%

difficulty of inconsistent responses of single response optimization. The range and goals of input variables i.e. SL, MC, and RM and the responses i.e. FS, Por. and DE are given in Table 4.

Optimization aims to evaluate the best set of inputs for maximization of flexural strength and porosity and minimization of dielectric constant. This is indicated by the desirability of RSM analysis. The optimum value of responses is to be chosen for the maximum desirability index for various sets of inputs. A set of 10 optimal solutions is derived and tabulated in Table 5 for the specific set of input range (Table 4). The desirability of output responses i.e., FS, Por. and DE is shown in Fig. 11 as a ramp graph. The desirability of each parameter and each response and combined parameters are shown in Fig. 12 as a bar graph. The overall desirability of the responses is found to be 0.803.

5.4.5 Confirmation Tests

The values of responses i.e., flexural strength, porosity and dielectric constant obtained by experimental runs are compared with predicted regression models for flexural strength, porosity, and dielectric constant for SiO_2-Si_3N_4 ceramic composite. The error between experimental and predicted values is predicted in Table 6 for all responses. It is found that a maximum error of ±3.10% in flexural strength, ±3.03% in porosity and ± 3.05% in dielectric constant existing. Hence it can be declared that the predicted models are confirming with experimental values. Hence the tests are confirmed and recommended that the models are accurate.

6 Conclusions

The following conclusions were drawn from the present work,

a) Fused silica (SiO_2) based ceramic composites SiO_2–Si_3N_4 have been successfully produced using the gel-casting method
b) The rheological behaviour of the SiO_2 suspensions including SiO_2–Si_3N_4 by varying dispersant content, pH value and solid loading have been thoroughly studied and useful ranges of solid loading (SL), monomer content (MC), the ratio of monomers (RM) and Si_3N_4 contents were decided based on initial experiments and they were as follows.

   i. Solid loading: 42 to 50 vol% for SiO_2-Si_3N_4
   ii. Monomer content: 10 to 15 wt%
   iii. The ratio of monomers: 3 to 7
   iv. Si_3N_4 content: 5 to 15 wt%

c) Darvan 821A is recommended as a dispersant and a dosage of 0.5 wt% showed better results over other dispersants in the suspension of ceramic particles as 0.5 wt% Darvan 821A gives the maximum zeta potential value for all SiO_2 suspensions.
d) The regression models for the analysis of responses such as FS, Por., and DE are developed and the effects of the process variables on these responses are studied.
e) The optimum process parameters for maximum FS, maximum Por., and minimum DE were evaluated using RSM coupled with desirability function to optimize multiple responses.

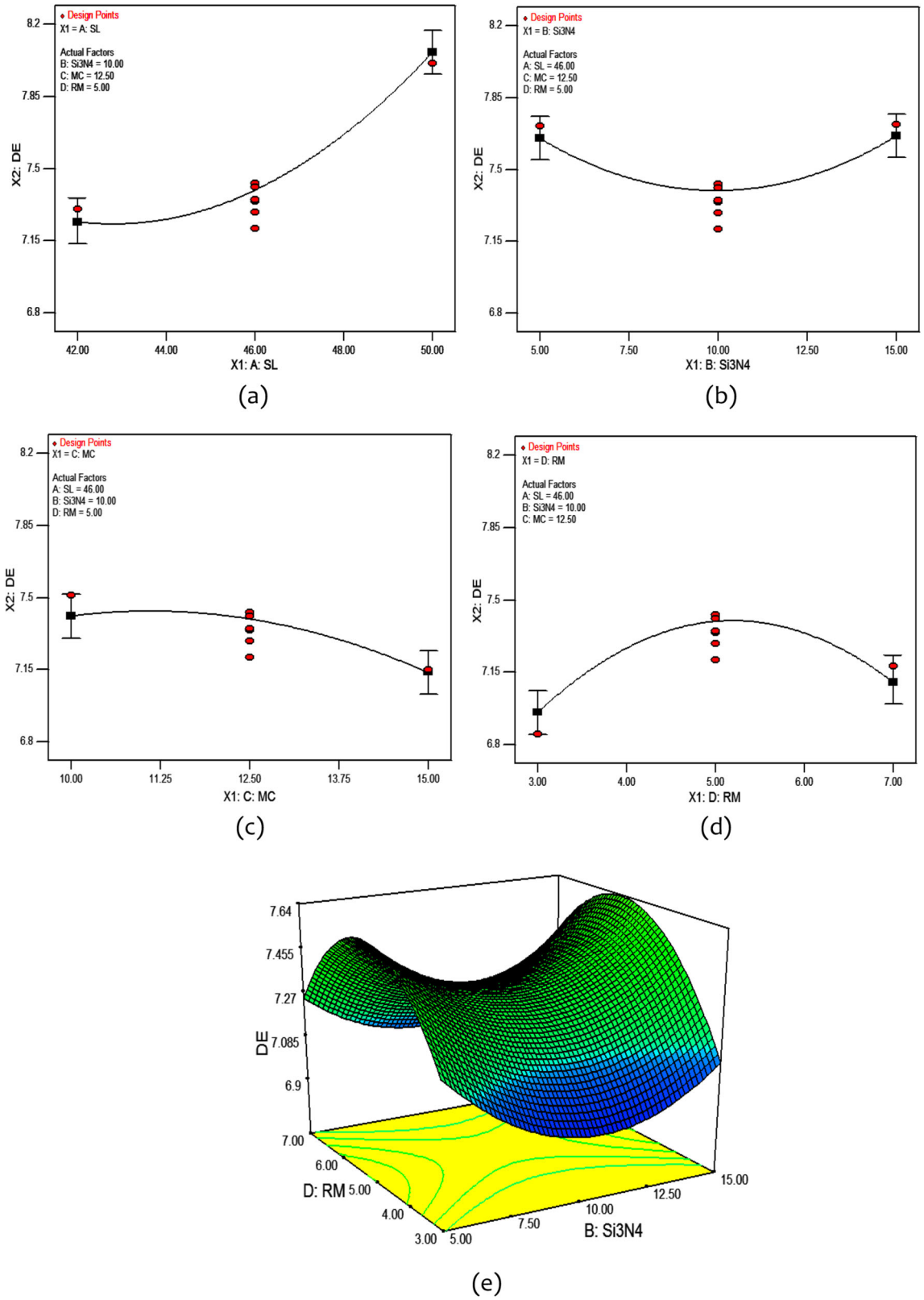

Fig. 10 Influence of process parameters on dielectric constant - (**a**) Influence of SL on DE, (**b**) Influence of Si3N4 on DE, (**c**) Influence of MC on DE, (**d**) Influence of RM on DE, and (e). Influence of Si3N4 and RM on DE

Table 4 Range of input variables and responses

Name	Goal	Lower Limit	Upper Limit
A-SL (vol%)	Maximize	42	50
B-Si_3N_4 content (wt%)	in range	5	15
C-MC (wt%)	is in range	10	15
D-RM	is in range	3	7
FS (MPa)	Maximize	56.19	95.12
Por. (%)	Maximize	31.95	41.28
DE	Minimize	6.8	8.14

Table 5 Set of optimal solutions for SiO_2-Si_3N_4 ceramic composite

Number	SL	Si_3N_4	MC	RM	FS	Por.	DE	Desirability
1	47.95	10.43	15	3	86.173	39.767	6.949	0.808
2	47.95	10.33	15	3	86.107	39.777	6.948	0.808
3	47.91	10.34	14.97	3	85.998	39.780	6.947	0.806
4	47.93	11.12	15	3	86.580	39.670	6.957	0.806
5	47.92	11.26	15	3	86.644	39.649	6.958	0.806
6	47.82	11.37	15	3	86.493	39.705	6.944	0.805
7	47.86	9.29	15	3	85.233	39.866	6.938	0.803
8	47.65	10.47	15	3.06	85.627	39.862	6.927	0.800
9	47.38	9.3	14.86	3	83.894	40.101	6.887	0.791
10	47.27	12.51	15	3	85.994	39.763	6.907	0.790

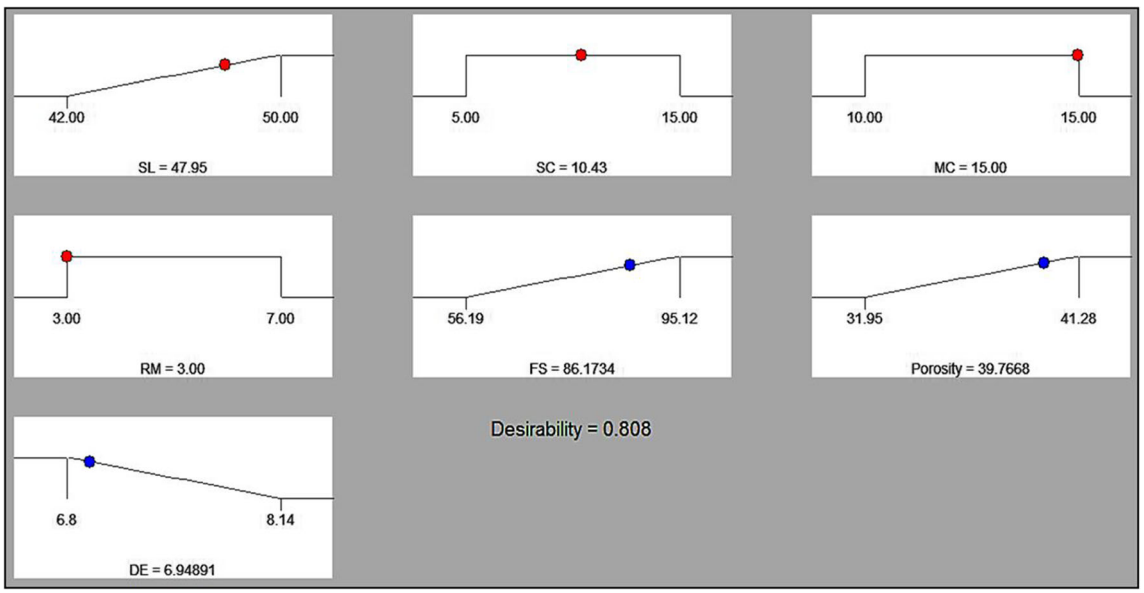

Fig. 11 Ramp graphs of desirability function for SiO2-Si3N4 ceramic composite

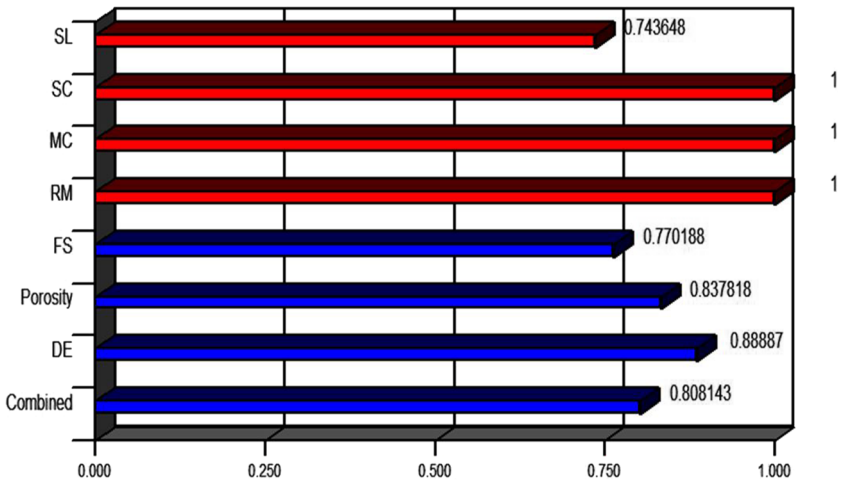

Fig. 12 Bar graphs of desirability function for SiO2-Si3N4 ceramic composite

Table 6. Error between experimental and predicted values

Run order	SL (vol%)	Si_3N_4 (wt %)	MC (wt %)	RM	Flexural Strength (MPa)			Porosity (%)			Dielectric Constant (K)		
					Expt.	Pred.	Error	Expt.	Pred.	Error	Expt.	Pred.	Error
1	42	5	10	3	56.19	54.98	2.15	37.53	37.71	-0.48	7.22	7.20	0.21
2	46	10	12.5	7	83.16	81.06	2.53	37.18	37.98	-2.15	7.32	7.10	3.06
3	50	15	10	3	92.66	92.24	0.46	32.61	32.09	1.59	7.81	7.78	0.37
4	42	15	10	3	67.89	67.35	0.79	38.41	38.58	-0.45	6.95	6.96	-0.11
5	46	5	12.5	5	75.02	76.46	-1.92	34.16	35.20	-3.04	7.71	7.65	0.78
6	42	5	15	3	58.13	59.49	-2.34	40.36	40.32	0.09	6.82	6.79	0.39
7	42	15	15	7	70.69	71.37	-0.97	38.94	38.46	1.24	6.89	6.95	-0.90
8	46	10	12.5	5	82.67	80.59	2.51	37.67	37.05	1.64	7.29	7.39	-1.40
9	46	10	12.5	3	76.15	78.32	-2.85	39.82	39.36	1.16	6.85	6.95	-1.49
10	42	15	15	3	69.15	68.95	0.29	41.28	41.20	0.20	6.80	6.79	0.20
11	46	15	12.5	5	85.16	84.79	0.44	35.87	35.17	1.96	7.72	7.66	0.80
12	50	5	15	7	89.36	90.22	-0.97	35.13	34.38	2.13	7.76	7.77	-0.14
13	50	15	15	7	93.88	94.50	-0.66	33.15	33.45	-0.90	7.81	7.78	0.44
14	46	10	12.5	5	80.98	80.59	0.48	36.59	37.05	-1.27	7.35	7.39	-0.58
15	50	15	10	7	95.12	94.09	1.09	31.95	32.07	-0.39	8.14	8.17	-0.41

f) The values of responses i.e., FS, Por., and DE obtained by experimental runs are compared with predicted regression models for FS, Por., and DE for SiO_2-Si_3N_4 ceramic composites.

Availability of Data and Material (data transparency) NA.
Code Availability (software application or custom code) NA.

Funding Nil

Declarations Additional declarations for articles in life science journals that report the results of studies involving humans and/or animals.

Ethics Approval (include appropriate approvals or waivers) NA.

Consent to Participate (include appropriate statements) Yes.

Consent for Publication (include appropriate statements) All authors have consented.

Conflicts of Interest/Competing Interests Nil

References

1. Li D, Zhang C, Li B, Cao F, Wang S, Yang B, Liu K (2012) Effects of oxidation treatment on properties of SiO_{2f}/SiO_2-BN composites. J Cent South Univ 19:30–35
2. Li F, Chen HY, Wu RZ, Sun BD (2004) Effect of polyethylene glycol on the surface exfoliation of SiC green bodies prepared by gelcasting. Mater Sci Eng A 368:255–259
3. Wan W, Huang C, Yang J, Zeng J, Qiu T (2014a) Effect of sintering temperature on the properties of fused silica ceramics prepared by Gelcasting. J Electron Mater 43:2566–2572
4. Haris JN, Welsh EA (1973) Fused Silica Design Manual, AD-766494
5. Jong BW, Slavens GJ, Traut DE (1992) Synthesis of silicon and silicon nitride powders by vapour-phase reactions. J Mater Sci 27(22):6086–6090
6. Chen F, Shen Q, Zhang L (2010) Electromagnetic optimal design and preparation of broadband ceramic radome material with graded porous structure. Prog Electromagn Res 105:445–461
7. Greil P (1989) Processing of silicon nitride ceramics. Mater Sci Eng 109:27–35
8. Omatete OO, Janney MA, Nunn SD (1997) Gelcasting: from laboratory development toward industrial production. J Eur Ceram Soc 17:407–413
9. Omatete OO, Janney MA, Strehlow RA (1991) Gelcasting - a new ceramic forming process. Am Ceram Soc Bull 70:1641–1649
10. Nojoomi A, Faghihi-Sani MA, Khoshkalam M (2014) Shear-rate dependence modeling of gelcast slurries: effects of dispersant content and solid loading. Ceram Int 40:123–128
11. Wan W, Yang J, Zeng J, Yao L, Qiu T (2014) Effect of solid loading on gelcasting of silica ceramics using DMAA. Ceram Int 40:1735–1740
12. Wan W, Yang J, Qiu T, Huang C (2014b) Study on Gelcasting of fused silica glass using glutinous Rice flour as binder. Int J Appl Glas Sci 5:401–409
13. Manivannan R, Kumar A, Subrahmanyam C (2013) Aqueous Gelcasting of fused silica using colloidal silica binder. J Am Ceram Soc 96:2432–2436
14. Mao X, Wang S, Shimai S (2006) Preparation of porous silica ceramics with low dielectric constant. Chin J Aeronaut 19:S239–S243
15. Lin S, Ye F, Ma J, Ding J, Yang C, Dong S (2016) Fabrication of multilayer electronic magnetic window material by Si_2N_2O decomposition. Mater Des 97:51–55
16. Jia DC, Zhou Y, Lei TC (2003) Ambient and elevated temperature mechanical properties of hot-pressed fused silica matrix composite. J Eur Ceram Soc 23:801–808
17. Zou C, Zhang C, Li B, Cao F, Wang S (2012) Improved properties and microstructure of porous silicon nitride/silicon oxide composites prepared by sol–gel route. Mater Sci Eng, A 556:648–652
18. Li X, Yin X, Zhang L, Cheng L, Qi Y (2009) Mechanical and dielectric properties of porous Si_3N_4–SiO_2 composite ceramics. Mater Sci Eng A 500:63–69
19. Ganesh I, Sundararajan G (2010) Hydrolysis-induced aqueous gelcasting of β-SiAlON–SiO2 ceramic composites: the effect of AlN additive. J Am Ceram Soc 93:3180–3189
20. Montgomery DG (2012) Design and analysis of experiments8th edn. John Wiley & Sons, New York
21. Box GEP, Draper NR (1987) Empirical model building and response surfaces. John Wiley & Sons, New York
22. Punugupati G, Bose PSC, Raghavendra G, Rao CSP (2020) Response surface modeling and optimization of Gelcast fused silica micro hybrid ceramic composites. Silicon 12(7):1513–1528